ISSN 0029 - 3865

CBPF-NF-004/86

STRUCTURE AND KINETICS OF FORMATION OF THE GEL PHASE IN HYDRATED TRICALCIUM SILICATE

by

Dimas R. Vollet[1] and Aldo F. Craievich

Centro Brasileiro de Pesquisas Físicas - CBPF/CNPq
Rua Dr. Xavier Sigaud, 150
22290 - Rio de Janeiro, RJ - Brasil

[1]Instituto de Química de Araraquara, UNESP
14.800 - Araraquara, SP - Brasil

ABSTRACT

The hydration of tricalcium silicate has been studied by small-angle X-ray scattering (SAXS) at different temperatures. The degree of hydration was determined by quantitative X-ray diffraction analysis (QXDA). The kinetics of setting of the pastes is well described by the Johnson-Mehl equation with $n = 2$, suggesting that the scattering objects (hydrated regions) grow by a diffusion controlled mechanism and have a shape of plates of constant thickness. Features of the SAXS curves from samples, in saturated conditions, are consistent with the lamellar model for the structure of the C-S-H gel.

Key-words: Tricalcium silicate; Hydration; SAXS.

1 INTRODUCTION

The products developed during the hydration of tricalcium silicate (C_3S) and Portland cement have similar properties [1, 2]. The basic ones are $Ca(OH)_2$ and a calcium silicate hydrate, called C-S-H, with typical structural features of a poorly crystallized material, often considered as a gel [1]. The fully hydrated paste also contains spaces which are water filled in the fresh paste [1]. These spaces become capilar pores [1] or inter-particles gel pores [3]. Because of their large size, their contribution to small-angle X-ray scattering (SAXS), in the accessible experimental angular range, is negligible.

The C-S-H phase has a characteristic structure containing very small pores, which is about 28% of the hydration products volume [4] and gives an important contribution to SAXS [2,5,6] The small pores are classified as intercrystallite or intracrystallite ones if they are, recpectively, external or internal to the "crystals" of the gel particles. The collapse of the interlayer spaces in a lamellar structure, during the drying process, is postulated by many authors [3,7,8,9,10]. However, there is some controversy about the reversibility of this process and its implications, mainly over the real value of the specific surface of the pastes and the methods for its determination [8,9,10,11].

The specific surface measurements by adsorption methods, and therefore in dry conditions, give values lower than $50m^2/g$ if N_2 is used as adsorbate [8], and of about $200m^2/g$ if water vapour is used [4,7]. The values obtained by Winslow and

Diamond [2] by SAXS in D-drying condition, are in agreement with those obtained by water vapour adsorption, under the same conditions but, in saturated conditions, the values are much greater ($\sim 700 m^2/g$) than those obtained by adsorption. These authors also showed that the specific surface decreases as drying progresses and that the loss is fully recovered by posterior resaturation, as long as the pastes have not been heated. They tried to associate the different values of the specific surface with the progressive collapse of the interlayers during drying, but verified that it is not at all clear that X-ray scattering measurements could record the interfaces between parallel adjacent layers. They concluded that a layer model is not necessarily appropriate for the C-S-H gel.

In this work, the kinetics of formation of the gel phase, developed during the hydration of C_3S, at several temperatures and the parameters associated with the gel structure of the saturated state and its changes during the drying processes, are studied.

2 EXPERIMENTAL PROCEDURE

Synthetic and microgranulated C_3S was mixed with distilled water in a water/solid weight ratio (w/c) of 0.5, molded into a sealed support and studied by SAXS for different hydration times at constant temperatures. Similar samples were studied by QXDA, using powdered Si as an internal standard and a Guinier chamber. The hydration degree was determined

from the decreasing in intensity of a set of diffraction lines of anhydrous C_3S, using a microdensitometer with integrator and record system.

The SAXS measurements were carried out using Cukα radiation and Kratky collimation, which gives a "linear and infinite" beam cross-section, a position sensitive X-ray detector and a multichannel analyser for data recording.

The SAXS data were analysed mainly using Porod's law that holds for two-electronic density (ρ_1 and ρ_2) systems, which correspond respectively to the ϕ and $(1-\phi)$ fractions of the total volume V. Using a "linear and infinite" beam cross-section, the asymptotic dependence of the scattering intensity, J(h), for such a system, is given by [12]:

$$\lim_{h\to\infty} J(h) = a/h3 \qquad (1)$$

where

$$a = \lim_{h\to\infty} J(h)h^3 = \pi^2(\Delta\rho)^2 S \qquad (2)$$

is Porod's law constant, $\Delta\rho = \rho_1 - \rho_2$, S is the total interphase area, and $\underline{h}$ the modulus of the scattering vector defined by $h = 4\pi \sin(\varepsilon/2)/\lambda$, where ε is the scattering angle and λ the incident radiation wavelength.

The SAXS data are often measured in relative units. In this case one determines the J(h)/Q ratio, where Q is the integrated scattering intensity over the reciprocal space, defined by [12]:

$$Q = \int_0^\infty J(h)h\,dh = 4\pi^2\phi(1-\phi)(\Delta\rho)^2V \qquad (3)$$

From (2) and (3) it follows

$$S/V = 4\phi(1-\phi)a/Q \qquad (4)$$

where S/V is the interphase area por unit volume of the sample.

In addition, from the S/V value one can determine the ℓ_1 and ℓ_2 parameters which represent a mean size of each phase. These parameters are averages of the intersection lenght, in the respective phases, of lines through all the points in all directions [12]:

$$\ell_1 = 4\phi V/S \quad ; \quad \ell_2 = 4(1-\phi)V/S \qquad (5)$$

Systematic deviations from Porod's law can occur when there are electronic fluctuations in the phases (positive deviation) or when the interphase is not well defined (negative deviation) [13]. In the first one, the corresponding intensity component, which is a function of the kind of fluctuations, and the scattering of the ideal two-density system, are simply additive. It results [13]:

$$J(h) = (a/h^3) + b_U/h \qquad (6)$$

$$J(h) = (a/h^3) + b_T \qquad (7)$$

for one-dimensional and tri-dimensional fluctuations, respectively, where the b parameters are related to the magnitude of fluctuations. Two-dimensional fluctuations were not observed in real systems. Tridimensional and one-dimensional fluctuations can be studied through $J(h)h^3$ vs. h^3 or h^2 plots, respectively. In both cases, a linear behavior should be observed in the Porod region. The slope of the straight line gives the b parameter and the extrapolation toward $h=0$ yields the a parameter.

3 EXPERIMENTAL RESULTS

3.1 SAXS

Fig. 1a shows the evolution of SAXS curves for several hydration times at 35°C. Fig. 1b shows the time evolution of the scattering intensity for various fixed h values. The time variations are similar for the various h values. The observed intensity increase is related to the paste setting when about 30 per cent of the hydration products is formed. The intensity change is proportional to the amount of the hydrated phase since the submicroscopic porous structure of the resulting C-S-H gel gives most of the contribution to SAXS.

Fig. 2 shows the time evolution of the C_3S transformed fraction, at 35°C, obtained by QXDA, and the changes in SAXS intensity for fixed h, obtained from samples sealed in dif

ferent conditions. The second and apparent increase of SAXS for the curve F is not associated with any corresponding evolution in the hydration degree. This intensity change is probably related [6] to an eventual water evaporation process leading to inhomogeneous emptying of the gel porosity and, consequently, to an enhancement of electronic contrast $(\rho_1-\rho_2)$. This conclusion seems to be confirmed by the analysis of a second sample (curve G) which shows such an effect just when the sealing of the system was removed (time ζ in Fig. 2).

The results shown in Fig. 2 indicate that the small-angle X-ray scattering intensity at fixed angles, from samples in saturated conditions, can be used in kinetic studies as a measure of the hydrated fraction.

3.2 Hydration kinetics

Curves like those of Fig. 1b were obtained at several temperatures. These curves suggest an analytical form like the Johnson-Mehl equation [14], to describe the SAXS evolution during the pastes setting stage:

$$(J_\infty - J_t) = (J_\infty - J_0)\exp(-k^n t^n/n) \qquad (8)$$

where J_t, J_0 and J_∞ are the scattering intensity values, respectively, at time t, extrapolated to $t = 0$ and corresponding to the apparent upper asymptote. k is an empirical velocity constant and n a parameter that is a function of the phase transformation determinant mechanism [14]. The $\ln\ln[(J_\infty-J_0)/(J_\infty-J_t)]$ vs.

ℓn t plot must be linear in this range, with a slope n. Fig. 3 shows it for several temperatures, yielding all of them $n \simeq 2$. Then, the k constants were obtained through the $\ln(J_\infty - J_t)$ vs. t^2 plots (Table I).

Fig. 4 shows the fitting of the Johnson-Mehl function (continuous line) with the experimental data. Excluding the region of higher temperatures, the plot of ln k vs. 1/T is linear (Fig. 5), fitting the Arrhenius law $k \propto \exp(-\Delta E/RT)$, where ΔE is the empirical activation energy of the process and R the gas constant. The slope gives $\Delta E = 37.2$ KJ/mol.

When the transformation occurs by growing of lamellar zones (constant thickness disks), an exponent n = 2 Johnson-Mehl equation, is expected [14].

3.3 Structural parameters and surface area of saturated gels

A positive deviation from Porod's law has been observed in SAXS curves corresponding to every sample in all stages of hydration. Fig. 6 shows a typical example, which corresponds to saturated conditions. Fig.7 shows the time evolution of a (surface parameter), b_T (fluctuation parameter), Q and a/Q ratio, during the paste setting at 35°C. There is a close relationship between the hydration degree (Fig. 2), Q, which is proportional to the amount of transformated phase, and a, which is proportional to the interphase area [equation (2)].

The a/Q ratio remains approximately constant. This suggests that the interphase area is approximately equivalent for all gel volume unity formed in this stage. Under these

conditions, one may write:

$$\phi_i = \alpha_i \phi_{gel} \tag{9}$$

and

$$a_i = \alpha_i a_{gel} \tag{10}$$

where ϕ_i and a_i are the volume fractions occupied by the gel pores and the surface parameter, respectively, corresponding to the hydration degree α_i and ϕ_{gel} and a_{gel} are the respective values corresponding to total hydration. By using equation (3), (9) and (10) one can extrapolate, from the measured values a/Q_i and α_i, the specific surface S/V for the gel phase (here taken as the whole hydration product and so $\phi_{gel} = 0.28$) [4]. Equation (4) can be written as follows:

$$(S/V)_{gel} = 4\phi_{gel}(1 - \alpha_i \phi_{gel}) a_i/Q_i \tag{11}$$

ϕ_{gel} excludes the coarse capillary porosity, which gives no contribution to SAXS, and includes every interlayer space. Equation (11) has not a strong dependence of α_i and errors on this parameter have little influence on the specific surface of the gel.

Table IIa shows the results corresponding to several samples under saturated conditions after the paste setting period. The ℓ_p and ℓ_s parameters, related respectively to the pores and the solid gel particles, obtained from equation (5), are

also included in Table II.

3.4 Influence of drying

In Fig. 8 (a,b) a comparison is made between the SAXS curves for a sample (C, Table IIa) in saturated condition and after 15 days in $CaCl_2$ desiccant (C',Table IIb). The increase in intensity with drying, already cited in section 3.1, is more pronounced in the region of very small angles.

Table IIb shows the changes in the structural parameters associated with the drying process. Because the drying conditions of the samples A' and C' (Table IIb) are not very well defined, only qualitative aspects of this process are discussed from the presented experimental data. $(S/V)_{gel}$ for the desiccated states decreases regarding the saturated condition while the pores and the solid particle sizes grow. This may occur by a clustering of the particles and pores of the gel. It may also occur that the decreasing in a/Q be caused by changes in contrast due to heterogeneous water evaporation, which could start by the greatest pores. The scattered intensity is proportional to $(\Delta\rho)^2$, so that Q, defined in the whole $\underline{h}$ space, is more sensitive to contrast variations related to greater pores, than $\underline{a}$, defined for $h \to \infty$, where the contribution of these pores is smaller. If the last consideration is correct, the two electronic density model cannot be applied to middle drying stages.

4 DISCUSSION

4.1 Specific surface

The gel specific mean value is saturated conditions (Table IIa) is 1.40 nm^{-1}. Winslow and Diamond [2], using the same technique for 86%-hydrated cement paste with w/c = 0.4, in saturated conditions, obtained 708 m^2/(g ignited at 1050°C) or about 566 m^2(D-dried g). They whose that these values are similar to those of a paste prepared from alita (impure C_3S). Extrapolating to 100% hydration gives 659m^2/(D-dried g). Taking the density d=2.4g/cm^3 [4] one gets $(S/V)_{100\%} = 1.58$ nm^{-1}. This value is in good agreement with that of the present work (Table IIa). The slightly higher value obtained from data of Ref. 2 may be due to the method used to measure the volume which includes the capillary porosity. A lower value of $(S/V)_{100\%}$-1.31 nm^{-1} has been obtained [2] for a 78% hydrated paste with w/c = 0.3.

According to Powers [4], 79% is the maximum hydration for a w/c=0.3 paste, what would lead to complete elimination of the capillary porosity and consequently the second value would be more representative for the gel. The average value corresponding to the two pastes (1.45 nm^{-1}) is in better agreement with that of the present work.

The D-dried state seems to be well described by a two electronic density model: empty pores ($\rho = 0$) and solid gel particles ($\rho \neq 0$). The agreement between the present results and those obtained by Winslow and Diamond [2], in saturated con

ditions, makes possible the use of their D-dried condition data for the discussion about the features of the dry pastes. From the data of reference [2] (78% and 86% hydrated pastes), we obtained the specific surface at 100% hydration in D-dried conditions, which is equal to 0.448 nm^{-1}. From equation (5) this value leads to $\ell_p = 2,5$ nm and $\ell_s = 6.4$ nm (Table IIb) which are about three times the corresponding values in saturated conditions, indicating a clustering of the gel particles and pores.

4.2 Structural model

Powers [4] postulated a thin sheet of thickness T to describe the colloidal particles of gel of cement pastes in the D-dried state. This shape was suggested by electron microscopy observations. This author obtained T = 3.4 nm from the specific surface measured by water vapour adsorption.

The same result is obtained from our SAXS data. For a thin sheet model we have $T_S = \ell_s/2$ [12], and therefore ℓ_s = 6.4 nm (Table IIb) leads to $T_s = 3.2$ nm, in agreement with Powers [4], and $T_P = \ell_p/2 = 1.25$ nm. Every shape proposed for the particles leads always to the same value for the specific surface, i.e. $(S/V) = 4\phi_i(1/\ell_i)$; thus their shape must be deduced from other observations.

The hydration kinetic studies (sec. 3.2) lead to a parameter n = 2 which suggests that the gel growth is controlled by diffusion. The gel is produced by the formation and lateral growth of plates of constant thickness [14]. Ap-

plying this model of plates, the SAXS results (Table IIa) concerning the saturated state, yields $T_s = 1.0$ nm and $T_p = 0.40$ nm. This would correspond to about one layer of tobermorite type, separated by one or two monolayers of water, on the average.

The dependence on h of the SAXS intensity from saturated samples gives another evidence of the lamellar model. Using a linear and infinite X-ray beam cross-section, a system of infinitely narrow plates, with a infinitely large lateral area A, will scatter according to [12]:

$$\lim_{A\to\infty} J(h)h^3 = \pi^2 A(\Delta\rho)^2 T^2 h^2 \propto h^2 \qquad (12)$$

The $J(h)h^3$ vs. h^2 plot is linear through the origin; Fig. 9 shows it for the saturated sample Z (Table IIa) where equation (12) is verified for a large range of h (until about 3.9 nm^{-1}). For $h \geq 3.5/T$, T = minimum plate dimension [15], the classic Porod's law $J(h) \propto 1/h^3$ would also be verified. T = 0.65 nm is the minimum sheet thickness that could be accurately measured in the h range for Porod's law fittings like the one shown in Fig. 6. Since the obtained value of pore thickness for samples in saturated state was $T_p = 0.4$ nm, the linear behaviour of the plot jh^3 vs. h^3 in the $3.9\ nm^{-1} < h < 5.5\ nm^{-1}$ range (Fig. 6) should be considered as an approximated agreement with equation (7). Then the surface parameter a and, consequently, the obtained thicknesses, T_p and T_s, of plates for the saturated state should be taken as approximated values. For a more accurate determination of T_p and T_s of saturated samples, SAXS studies at higher angles would be necessary.

The experimental thickness of the lamellar particles and pores of the saturated gel ($T_s = 1.0$ nm and $T_p = 0.40$ nm) are clearly lower than those corresponding to D-dried state ($T_s = 3.2$ nm and $T_p = 1.25$ nm). This suggests a clustering, by drying, of three elementary layers, on the average, separated by the equivalent clustering of the interlayer spaces in the former saturated state. Some spherical and bigger pores could possibly be present here, even in the previous saturated state, but they may bring a smaller contribution to the specific surface. This contribution could be similar to that recorded by N_2 adsorption.

Water vapour adsorption and SAXS lead to the same surface for D-dried state, suggesting that water records the lateral interfaces of the clustered layers but, in the measurement conditions, it does not recover the interlayer spaces collapsed during the drying process.

5 CONCLUSION

The parameter $n = 2$ in the kinetic study of the C_3S transformation during hydration and the features of the small-angle X-ray scattering curves for the saturated conditions [$J(h) \propto 1/h$], allow to conclude that the C-S-H gel exhibits a lamellar morphology.

The increase in T_s and T_p on passing from the saturated to the dry condition indicates that most of the elementary C-S-H lamellas coalesce, increasing the T_s and T_p thickness,

without a substantial modification of the global lamellar gel structure observed by electronic microscopy. The increase in the solid sheet thickness and the clustering of the empty lamellar spaces would lead to a coarser structure without an appreciable change in the total volume of the gel.

FIGURE CAPTIONS

Fig. 1 - a) SAXS curves for several hydration times
o : 1.0h, Δ : 8.0h, □ : 26h.
b) SAXS intensity as a function of hydration time at various $\underline{h}_o$ values o : 0.78nm^{-1}, □ : 1.53nm^{-1}, Δ : 2.14nm^{-1}.

Fig. 2 - Hydration degree (QXDA) and variation of SAXS intensity at 35°C, o : QXDA, Δ and □ : SAXS intensity under F and G conditions respectively (see text).

Fig. 3 - Johnson-Mehl plots at various temperatures.
a : 25°C (n = 2.09); b : 35°C (n = 2.01); c : 44°C (n = 2.01); d : 52°C (n = 2.04); e : 65°C (n = 2.03).

Fig. 4 - Fitting of Johnson-Mehl equation. ● : 25°C, x : 35°C, ▲ : 44°C, □ : 52°C, o : 65°C.

Fig. 5 - Arrhenius plot for the empirical hydration velocity.

Fig. 6 - Typical Porod plot indicating a linear region in agreement with equation 7.

Fig. 7 - Hydration kinetic parameters. ϕ : a/Q ratio, □ : integrated intensity (Q) (the continuous line represents the Johnson-Mehl function), + : fluctuation parameter (b), o : surface parameter (a).

Fig. 8 - Effects of drying on the SAXS intensity. o : saturated state, □ : 15 days under $CaCl_2$ desiccant. a) J vs. h plot, b) Jh^3 vs. h^2 plot.

Fig. 9 - SAXS intensity from a saturated sample showing the behavior expected from lamellar systems ($h^* = 3.9\,mm^{-1}$).

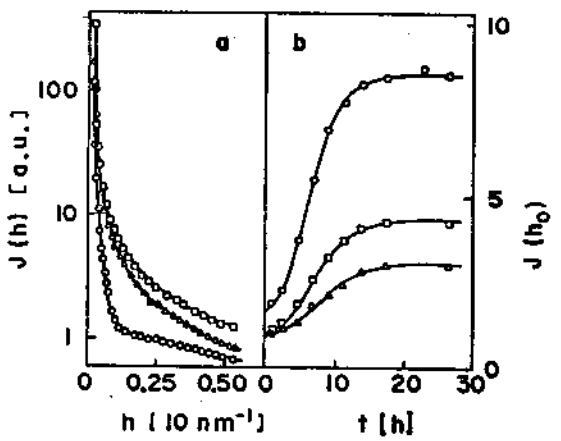

FIG. 1

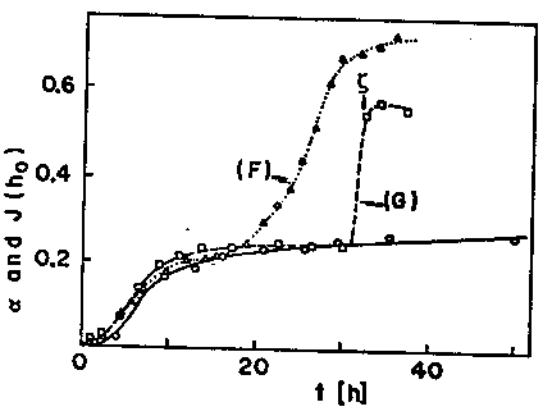

FIG. 2

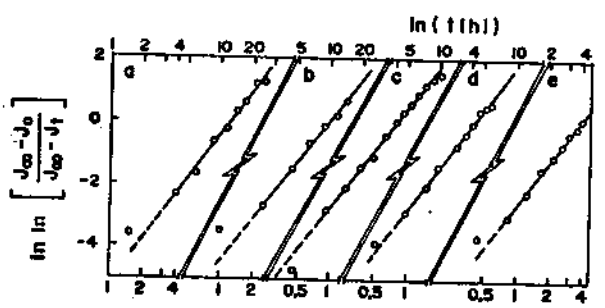

FIG. 3

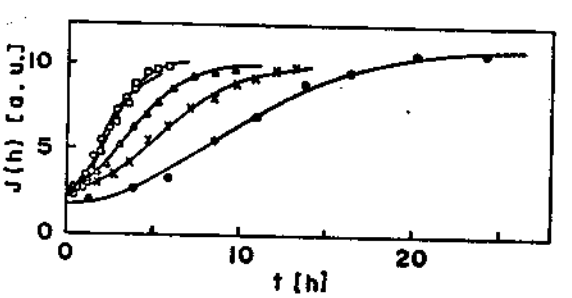

FIG. 4

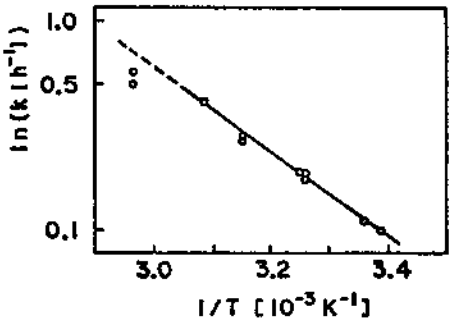

FIG. 5

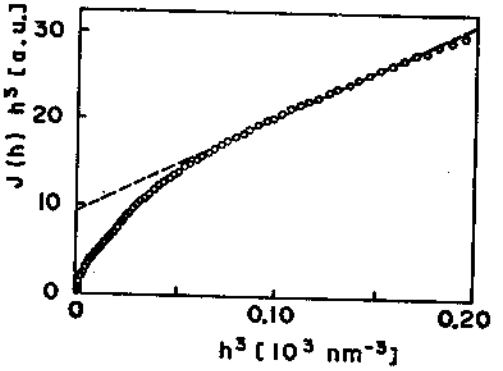

FIG. 6

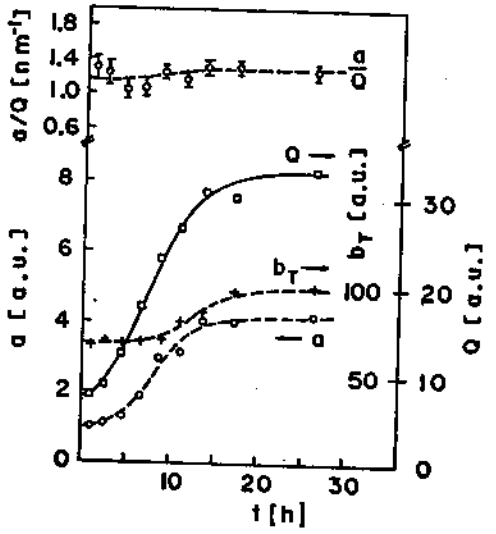

FIG. 7

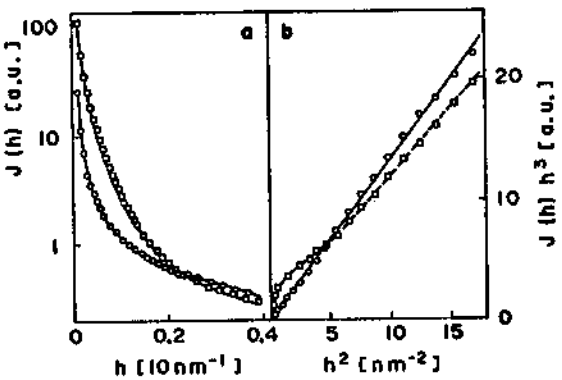
a
b
100
10
1
J (h) [a.u.]
0
0.2
0.4
h [10nm⁻¹]
5
10
15
h² [nm⁻²]
20
10
0
J (h) h³ [a.u.]

FIG. 8

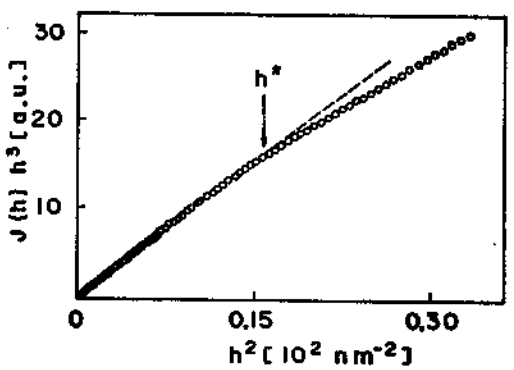
30
20
10
J (h) h³ [a.u.]
h*
0
0.15
0.30
h² [10² nm⁻²]

FIG. 9

TABLE I

Empirical velocity constant

T(^{0}C)	k(h^{-1})	T(^{0}C)	k(h^{-1})
22	0.103	44	0.287
25	0.117	44*	0.283
34	0.198	52	0.442
34*	0.181	65	0.496
35	0.196	65*	0.565

(*) Replica

TABLE IIa

Results for saturated samples.

Sample	Conditions	α_i	a_i/Q_i (nm^{-1})	(S/V)gel (nm^{-1})	ℓ_p (nm)	ℓ_s (nm)
A	35°C satur.	0.28	1.32	1.36	0.82	2.1
B	25°C satur.	0.32	1.38	1.41	0.79	2.0
C	25°C satur.	0.45	1.47	1.44	0.78	2.0
Z	25°C satur.	0.70	1.53	1.38	0.81	2.1

TABLE IIB

Results for dried samples

A'	35°C, after removal of the sealing of the system	0.30	0.780	0.800	1.4	3.6
C'	Sample C, 15 days in $CaCl_2$ desiccant	0.45	0.677	0.663	1.7	4.3
WD	D-dried, average of two pastes from ref (2)	0.78-0.86		0.448*	2.5	6.4

(*) Estimated value from the data in Ref. (2)

REFERENCES

1. T.C. POWERS (1958), "Structure and Physical Properties of Hardened Portland Cement Paste", J. Am. Cer. Soc. 41, 1-6.
2. D.N. WINSLOW and S. DIAMOND (1974), "Specific Surface of Hardened Portland Cement Paste as Determined by Small-Angle X-ray Scattering", J. Am. Cer. Soc. 57, 193-197.
3. M. DAIMON, S.A. EBO-EL-ENEIN, G. HOSAKA, S. GOTO and R. KONDO (1977), "Pore Structure of Calcium Silicate Hydrate in Hydrated Tricalcium Silicate", J. Am. Cer. Soc. 60, 110-114.
4. T.C. POWERS (1964), "Physical Structure of the Portland Cement Paste", in The Chemistry of Cements, by H.F.W. Taylor, Academic Press, London, Vol. I, p.444.
5. D. VOLLET, A. CRAIEVICH and M. REGOURD (1984), "Small Angle X-Ray Scattering from Hydrating Tricalcium Silicate", J. Amer. Cer. Soc., 67, 315-318.
6. D. VOLLET and A. CRAIEVICH (1984), "Structural Transformations in the Hydrated Tricalcium Silicate" (in Port.), Proc. Sixty Brazilian Congress of Materials Science, Rio de Janeiro, T-6, pp. 24-29.
7. R. Sh. MIKHAIL, D.H. TURK and S. BRUNAUER, (1975), "Dimensions of the average Pore, the Number of Pores, and the Surface Area of Hardened Portland Cement Paste", Cem. Concr. Res., 5, 433-442.
8. P.J. SEREDA, R.F. FELDMAN and V.S. REMACHANDRAN (1980), "Porosity and Pore-Size Distribution in Ordinary Portland Cement Paste", Proc. Seventy Int. Congr. Chemistry of Cement, Paris, Vol. I, pp VI-1/10-21.

9. S. BRUNAUER, I. ODLER and M. YUDENFREUND (1970), "New Model for Hardened Portland Cement Paste", Highw. Res. Rec. 328, pp. 89-101, 105-107.

10. R.F. FELDMAN and P.J. SEREDA (1968), "Model for Hydrated Portland Cement Paste as Deduced from Sorption-Length Change and Mechanical Properties", Mater. Constr., 1, 509-520.

11. R.F. FELDMAN and V.S. RAMACHANDRAN (1971), "Differentiation of Interlayer and Adsorbed Water in Hydrated Portland Cement by Thermal Analysis", Cem. Concr. Res., 1, 607-620.

12. O. GLATTER and O. KRATKY (1982), Small-Angle X-ray Scattering, Academic Press, London.

13. W. RULAND (1971), "Small-Angle Scattering of two Phase Systems: Determination and Significance of Systematic Deviations from Porod's Law", J. Appl. Cryst. 4, 70-73.

14. J. BURKE (1965), Kinetics of Phase Transformations in Metals, Pergamon Press, London.

15. H.D. BALE and P.W. SCHMIDT (1984), "Small-Angle X-ray Scattering of Submicroscopic Porosity with Fractal Properties", Phys. Rev. Lett. 53, 596-599.